On the Formation of a Third, Nanostructured Domain in Ionic Liquids

ARTICLE *in* THE JOURNAL OF PHYSICAL CHEMISTRY B · AUGUST 2013

Impact Factor: 3.3 · DOI: 10.1021/jp402300c · Source: PubMed

THE JOURNAL OF PHYSICAL CHEMISTRY B

Article

pubs.acs.org/JPCB

On the Formation of a Third, Nanostructured Domain in Ionic Liquids

Ana B. Pereiro,*[,†] M. J. Pastoriza-Gallego,[‡] Karina Shimizu,[§] Isabel M. Marrucho,[†,∥] José N. Canongia Lopes,*[,†,§] Manuel M. Piñeiro,[‡] and Luis Paulo N. Rebelo[†]

[†]Instituto de Tecnologia Química e Biológica, Universidade Nova de Lisboa, Apartado 127, 2780-157 Oeiras, Portugal

[‡]Departamento de Física Aplicada, Facultade de Ciencias, Universidade de Vigo, E36310 Vigo, Spain

[§]Centro de Química Estrutural, IST/UTL, 1049 001 Lisboa, Portugal

[∥]Departamento de Química, CICECO, Universidade de Aveiro, 3810-193 Aveiro, Portugal

Supporting Information

ABSTRACT: The study of solid−fluid transitions in fluorinated ionic liquids using differential scanning calorimetry, rheology, and molecular modeling techniques is an essential step toward the understanding of their dynamics and the thermodynamics and the development of potential applications. Two fluorinated ionic liquids were studied: 1-hexyl-3-methylimidazolium perfluorobutanesulfonate, HMIm(PFBu)SO_3, and tetrabutylammonium perfluorobutanesulfonate, NB_4(PFBu)SO_3. The experimental calorimetric and rheological data were analyzed taking into account the possible mesoscale structure of the two fluorinated ionic liquids. The simulation results indicate the possible formation of three nanosegregated domains—polar, nonpolar, and fluorous—that may have a profound impact on ionic liquid research. In the case of HMIm(PFBu)SO_3 the three types of mesoscopic domains can act as interchangeable jigsaw pieces enabling the formation of multiple types of crystals and inducing the observed calorimetry and rheological trends.

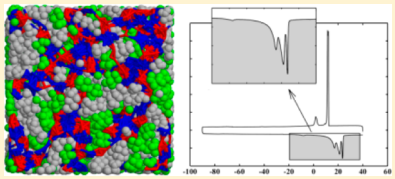

INTRODUCTION

Ionic liquids (ILs) have become a popular green media for engineering problems due to their physicochemical properties, leading to an exponential growth in the number of publications in this field. However, there are still many unexplored themes, such as the case of the fluorinated ionic liquids (FILs) family. The use of fully or partially fluorinated ionic liquids is of interest in areas where fluorinated organic compounds are applied as refrigerants, surfactants, and polymers as well as components of pharmaceuticals, fire retardants, lubricants, and insecticides.[1] Their potential as gas carriers, including possibly as synthetic blood substitutes[2] and as solubility promoters in supercritical extraction media,[3] has received considerable recent attention. This wide range of applications results from the unique properties of highly fluorous carbons, namely their high capacity for dissolving gases and low surface tension, low intensity interactions with normal organic compounds,[4] and outstanding chemical and biological inertness. The molecular structures of FILs can be dominated by the very strong C−F bonds, causing an increase in rigidity and a decrease in polarity.[5] This fact leads to high solubility and low energy requirements for expelling the molecules and regenerating the solvent upon either a decrease in pressure or/and an increase in temperature.

Although anions such as bis(trifluoromethylsulfonyl)imide, hexafluorophosphate, or tetrafluoroborate anions have been frequently characterized and denoted as conventional fluorinated ionic liquids, few works have dealt with the FILs family,[6−15] defined as ionic liquids with fluorous chain lengths equal to or greater than four carbon atoms. Thus, this work details with the behavior of FILs with longer fluorous chains that are distinct from conventional fluorinated ionic liquids, which have fewer than four carbons in the fluorous alkyl chain. The FILs research with longer fluorous chains has focused merely on synthesis and characterization as well as their application as reaction media and as materials.[8−15] No deep and precise structural characterization of aprotic FIL (ionic liquids studied in this work) is available in the literature. Only two papers[6,7] have studied the self-assembly nanostructure of protic ionic liquids with fluorous anions using small- and wide-angle X-ray scattering. This intermediate range order results from segregation of the polar, nonpolar, and fluorous domains of these FILs. A structure−property relationship between the chemical structure and their liquid nanostructure has been established in one of these papers,[6] and the results show that ions in these FILs can be tailored to achieve specific intermediate range order length scales, modified to increase or decrease the intensity of the ordering.[6] Other paper[16] shows molecular dynamic simulations of FILs based on bis-(trifluoromethylsulfonyl)imide anion and on imidazolium cation with fluorous chains of variable length. This study reveals remarkably little influence of partial fluorination on the spherically averaged intermolecular structure of the FILs and little change in tail conformations and the extent of tail−tail aggregation upon partial fluorination.[16] It must be stressed that in that case the anion has two terminal CF_3 groups that can adopt different relative orientations while interacting with the partially fluorinated chains of the cation. This feature

Received: March 6, 2013
Revised: August 20, 2013
Published: August 21, 2013

(enhanced flexibility/complexity) has also been evidenced by the corresponding IL crystalline structures that are dominated by the conformations adopted by the anion.[17]

Nowadays, ILs are regarded as nanosegregated fluids, with a polar network permeated by nonpolar domains. This structural feature of ILs was first reported using all-atom simulations[18] by one member of our research group and was afterward corroborated by experimental techniques. Triolo et al.[19] provided the first experimental evidence of the existence of nanoscale heterogeneities in neat liquid and supercooled RTILs using X-ray diffraction. Furthermore, the nanostructured nature of many ILs has been established in recent years by different research groups.[19−24] This increased our understanding of the peculiar solvent behavior of ILs at a molecular level.[25] On the other hand, the formation of distinct hydrophobic and hydrophilic solvation fields has already been observed in the binary mixtures of small chain (up to 3 carbons) fluorinated alcohols and water and is due to the strong formation of fluorinated alcohol clusters and water clusters.[26] It is, thus, expected that the fluorous alkyl chain (with four carbons) in the FILs studied will also control the formation of fluorous nanodomains and may induce the formation of three nanosegregated domains: polar, nonpolar, and fluorous. With this aim in mind, two fluorinated ionic liquids (1-hexyl-3-methylimidazolium perfluorobutanesulfonate, HMIm(PFBu)-SO_3, and tetrabutylammonium perfluorobutanesulfonate, $NB_4(PFBu)SO_3$, were selected, and their structural characterization was carried out using differential scanning calorimetry (DSC) and rheology techniques. This characterization allows us to identify and locate the solid−fluid transitions of FILs and their dynamics and thermodynamic behavior. Molecular dynamic simulations of these fluorinated ionic liquids have also been performed in order to study nanoscale structuring and investigate the possible formation of three nanosegregated domains.

EXPERIMENTAL SECTION

Materials. Tetrabutylammonium perfluorobutanesulfonate, >98% mass fraction purity, halides (IC) <100 ppm, cation (IC) >99.75%, anion (IC) >99.72%, and 1-hexyl-3-methylimidazolium perfluorobutanesulfonate, >99% mass fraction purity, halides (IC) <250 ppm, cation (IC) >99%, anion (IC) >99%, were supplied by IoLiTec GmbH, and their chemical structure and respective abbreviations are depicted in Table S1 (see Supporting Information). Fluorinated ionic liquids were dried under vacuum (3×10^{-2} Torr) and vigorously stirred at 323.15 K for at least 2 days immediately prior to use. Water content, determined by Karl Fischer titration, was less than 100 ppm. No further purification of the ILs was carried out. The purity of the final products was checked by ^{1}H NMR.

Each fluorinated ionic liquid was taken from the respective Schlenk flask with a syringe under a nitrogen flow to prevent humidity and was immediately placed in the apparatuses.

Thermal Analysis. A DSC Q200 differential scanning calorimeter (TA Instruments) was used to measure the phase transitions of the fluorinated ionic liquids. Cooling was accomplished by a refrigerated cooling system capable of controlling the temperature down to 183.15 K. The sample was continuously purged with 50 mL min^{-1} dry dinitrogen gas. About 5−10 mg of fluorinated ionic liquid was crimped in an aluminum standard sample pan. Indium (mp, T = 429.76 K) was used as the standard compound for the calibration of the DSC. The fluorinated ionic liquid samples were cooled to 183.15 K and tempered (30 min) and finally heated to 313.15 K for $HMIm(PFBu)SO_3$ and 423.15 K for $NB_4(PFBu)SO_3$. The cooling−heating cycles were repeated three times at different rates (10, 5, and 1 K min^{-1}). The transition temperatures and enthalpies obtained from the second and subsequent cycles at the same rate were reproducible.

Rheological Analysis. The experimental device used was a Physica MCR 101 rheometer (Anton Paar, Graz, Austria), equipped with plate−plate geometry and Peltier temperature control. Further details of the experimental setup can be found in a previous work.[27]

Molecular Dynamic (MD) Simulations. In IL modeling and force field parameterization, the CLaP force field[28−30] with parameters specifically tailored to include entire ionic liquid homologous series was used to model all ions under consideration. The simulation runs were conducted using the DLPOLY package,[31] and the function has the general form given by eq 1:

$$u_{\alpha,\beta} = \sum_{ij}^{\text{bonds}} \frac{k_{ij}}{2}(r_{ij} - r_{0,ij})^2 + \sum_{ijk}^{\text{angles}} \frac{\theta_{ij}}{2}(\theta_{ijk} - \theta_{0,ijk})^2 + \sum_{ijkl}^{\text{dihedrals}} \sum_{m=1}^{4} \frac{V_{m,ijkl}}{2}[1 - (-1)^m \cos(m\phi_{ijkl})] + \sum_{ij}^{\text{nonbonded}} \left\{ 4\varepsilon_{ij}\left[\left(\frac{\sigma_{ij}}{r_{ij}}\right)^{12} - \left(\frac{\sigma_{ij}}{r_{ij}}\right)^{6}\right] + \frac{1}{4\pi\varepsilon_0}\frac{q_i q_j}{r_{ij}} \right\} \quad (1)$$

with the traditional decomposition of the potential energy, $u_{\alpha\beta}$, into covalent bond stretching, valence angle bending, torsion barriers around dihedral angles, and atom−atom pairwise repulsive, dispersive, and electrostatic contributions. The Coulomb interactions are defined in terms of atomic point charges while the (12−6) Lennard-Jones potential describes the repulsive and dispersive terms. Together they act either between sites in different molecules or between sites in the same molecule separated by three or more bonds. A scaling factor of 0.5 is applied to the Lennard-Jones and Coulombic interactions when sites in the same molecule are exactly three bonds apart.

In molecular dynamics and structure factors, all MD simulation runs representing each pure ionic liquid started from low-density initial configurations composed of 250 ion pairs for 1-hexyl-3-methylimidazolium perfluorobutanesulfonate ($HMIm(PFBu)SO_3$), 280 ion pairs for 1-hexyl-3-methylimidazolium butanesulfonate ($HMImBuSO_3$), 200 ion pairs for tetrabutylammonium perfluorobutanesulfonate ($NB_4(PFBu)SO_3$), and 230 ion pairs for tetrabutylammonium butanesulfonate (NB_4BuSO_3), yielding cubic simulation boxes of approximately 125 nm^3. The boxes were equilibrated in isothermal−isobaric ensemble conditions for 700 ps at 343 K using a Nosé-Hoover thermostat and an isotropic barostat with time constants of 0.5 and 2 ps, respectively, in order to achieve optimal convergence to the selected temperature and pressure set in the $N-p-T$ conditions. Further consecutive simulation runs of 1.5 ns each (total simulations times ranging from 6 to 9 ns) were used to produce equilibrated systems at the temperature studied. Electrostatic interactions were treated using the Ewald summation method considering six reciprocal-space vectors, and repulsive−dispersive interactions were explicitly calculated below a cutoff distance of 1.6 nm (long-

dx.doi.org/10.1021/jp402300c | J. Phys. Chem. B 2013, 117, 10826−10833

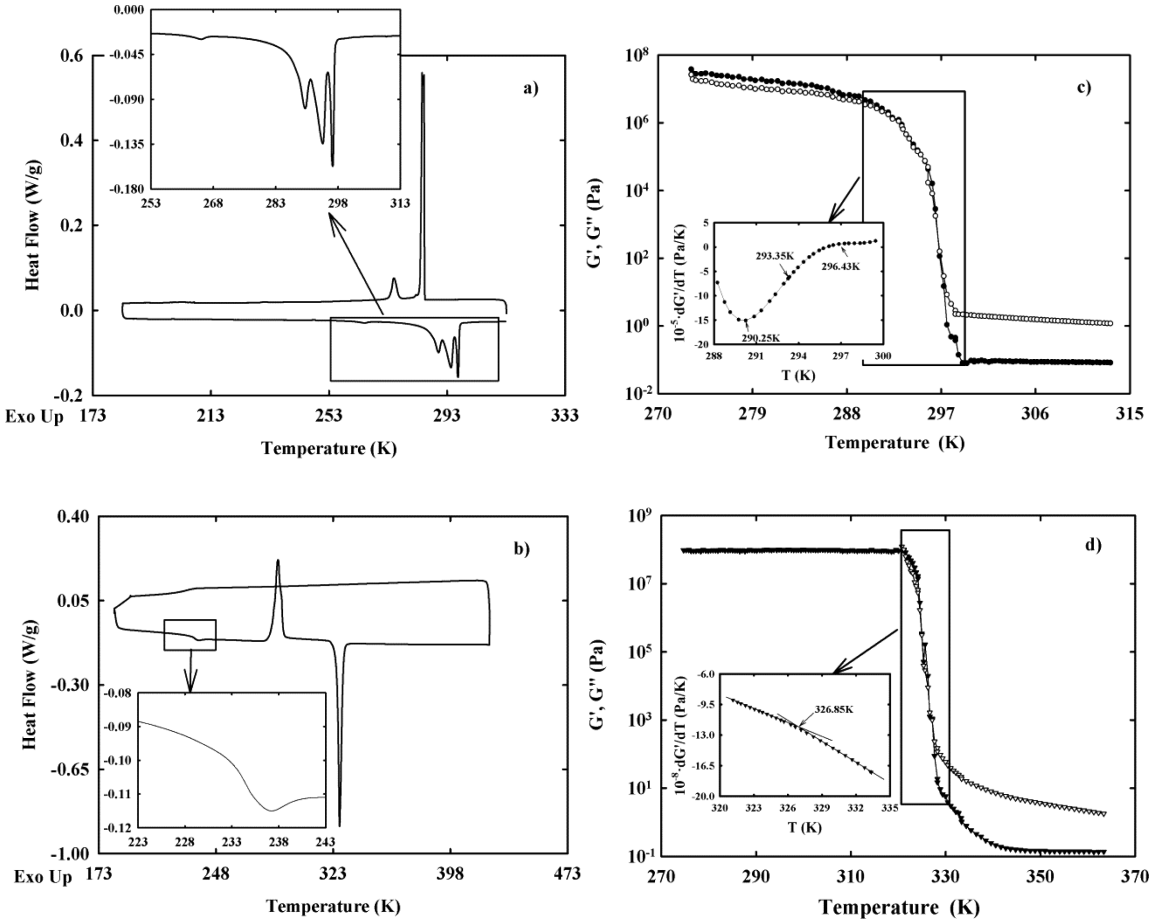

Figure 1. DSC curves for FILs: (a) HMIm(PFBu)SO_3 at a scan rate of 1 K min^{-1} and (b) NB_4(PFBu)SO_3 at a scan rate of 5 K min^{-1} and store (G', black symbols) and loss (G'', white symbols) moduli vs temperature measured at a fixed omega = 10 rad s^{-1}, and strains varying between 0.01% and 10% (ensuring its location within the LVR), for (c) HMIm(PFBu)SO_3 at a heating rate of 1 K min^{-1} and (d) NB_4(PFBu)SO_3 at a heating rate of 5 K min^{-1}.

range corrections were applied assuming uniform density beyond such cutoff radius).

The partial static structure factors, $S_{ij}(q)$, corresponding to the partial pair radial distribution functions of atoms i and j, $g_{ij}(r)$, were computed by Fourier transform according to eq 2:

$$S_{ij}(q) = \rho_0 \int_R^0 4\pi r^2[g_{ij}(r) - 1]\frac{\sin(qr)}{qr}\frac{\sin(\pi r/R)}{\pi r/R}\,dr \quad (2)$$

where ρ_0 is the average atom number density and R is the maximum value of the integration in real space which is set at half the size of the cubic simulation box side. To reduce the effect of fixed cutoff of fixed cutoff of r, a Lorch-type window function $(\sin(\pi r/R)/(\pi r/R))$ was added to eq 2.[32] To obtain the total static structure factors, the partial structure factors were combined in eq 3:

$$S(q) = (\sum_{i=1}^{n} x_i b_i)^{-2} \sum_{i,j=1}^{n} x_i x_j b_i b_j S_{ij}(q) \quad (3)$$

in which x_i and x_j are the corresponding atomic fraction and b_i and b_j are the atomic form factor.

RESULTS AND DISCUSSION

Thermal Analysis. Phase transitions were measured by DSC and thermal analysis curves for the two FILs are illustrated in Figure 1. The melting, glass transition, and solid−solid transition temperatures, together with transition enthalpies and DSC curves at all scan rates, are summarized in Table S2 and in Figures S1 and S2, respectively (see Supporting Information).

In the case of HMIm(PFBu)SO_3, four transitions at 265.04, 290.10, 294.33, and 296.75 K are reported from the heating cycle with a scan rate of 1 K min^{-1} (see Figure 1a). These several successive endothermic peaks correspond to three solid−solid phase transitions and the melting, respectively. The observed solid−solid transitions can be ascribed to different crystalline solids that can be formed due to the existence of three domains (polar, nonpolar, and fluorous) of potentially similar dimensions or can be due to conformational changes in the flexible cation $HMIm^+$.[33−35] From these results and taking in account the previous papers[6,7] where the persistent nanostructure in FILs has been demonstrated, it is also possible to conclude that, if one recognizes HMIm (PFBu)SO_3 as a strongly nanostructured fluid, the origin of such complex thermal behavior could also lie in the link between the multiple phase transitions and the possibility of cooperative conformational changes of the three domains in the fluorinated ionic liquid.

NB_4(PFBu)SO_3 remains liquid upon cooling (subcooled liquid state) until it reaches a glass transition at low temperature (see Figure 1b). The glass transition with enthalpic relaxation is reached at 234.45 K in the heating part of the cycle

dx.doi.org/10.1021/jp402300c | J. Phys. Chem. B 2013, 117, 10826−10833

at a scan speed of 5 K min^{-1}. Upon heating above the glass transition, $NB_4(PFBu)SO_3$ exhibits an exothermic crystallization peak at 287.70 K (cold crystallization temperature) followed by an endothermic melting peak at 327.13 K. This FIL shows thermal hysteresis.

Rheological Analysis. In order to obtain an alternative insight into the behavior of the solid fluid transition of these two FILs, a complete rheological study was performed at temperatures from 273 to 383 K. The trend of the viscoelastic properties of a fluid is directly correlated with the internal molecular structure, also reflecting all phase and structural changes. Rheological oscillatory experiments were thus performed to determine the viscoelastic behavior of both FILs. The power of dynamic testing is that the sample stress can be separated into its elastic and viscous contributions, and thus the elastic or storage modulus G' and the viscous or loss modulus G'' can be analyzed.

First, the linear viscosity range (LVR) was determined by performing strain sweep tests at several temperatures and at a constant angular frequency of ω = 10 rad s^{-1}. Then, a heating ramp within this LVR was performed, exploring the phase transition temperature range. Special care was taken to adjust the strain value for each temperature to ensure that the fluid consistently remained inside the LVR region. The results of G' and $G''$are displayed in Figures 1c and 1d. For the case of $HMIm(PFBu)SO_3$, within the solid region, G' slightly exceeds G'' as expected, and the trend in the solid−fluid transition region is very revealing. The inset in Figure 1c shows the derivative of G' with temperature (dG'/dT), a magnitude that shows change of trend for each structural change occurring within the fluid. This allows us to determine the position not only of the melting point but also two previous transitions, at the same temperatures (within the experimental uncertainty) as those observed by DSC. The nature of these solid−solid transitions cannot be ascertained using these experimental techniques, but some considerations can be discussed. First, it is well-known that perfluorinated chains are less flexible in their intramolecular configurations than their counterpart aliphatic chains. Also, previous results regarding the appearance or partially order domains in ILs containing long aliphatic chains[25,36] have suggested that these so-called solid−solid transitions might be produced by partial order transitions between liquid-crystal-like mesophases. The differing interactions between perfluorinated and aliphatic chains, which tend to group separately, could be the underlying reason for this rich phase transition scenario. The appearance of these transitions strongly supports the hypothesis of a nanostructure in FILs in the liquid phase. This hypothesis is supported by experimental results obtained by Shen et al.[6] that provided the segregation of the polar, nonpolar, and fluorous domains of the FILs. The difference between $HMIm(PFBu)SO_3$ and $NB_4(PFBu)SO_3$ is the flexible cation $HMIm^+$ which permits that the mesoscopic domains (polar, nonpolar, and fluorous) can act as interchangeable jigsaw pieces (the three domains have similar dimensions) or can exist conformational changes in this flexible cation.[33−35] In the case of NB_4 $(PFBu)SO_3$, the cation is symmetric with polar and nonpolar domain interlocked, and this fact can hinder the formation of multiple types of crystals.

Another interesting study is the angular frequency sweep at a fixed temperature and strain. In the case of a perfect solid, this should yield a constant value representation for G' with no viscous modulus G''. The results of this study are shown in Figure 2, and for the first FIL, it is clear that there is also a viscous modulus component, while both moduli are frequency dependent, which does not correspond to a perfect crystalline solid.

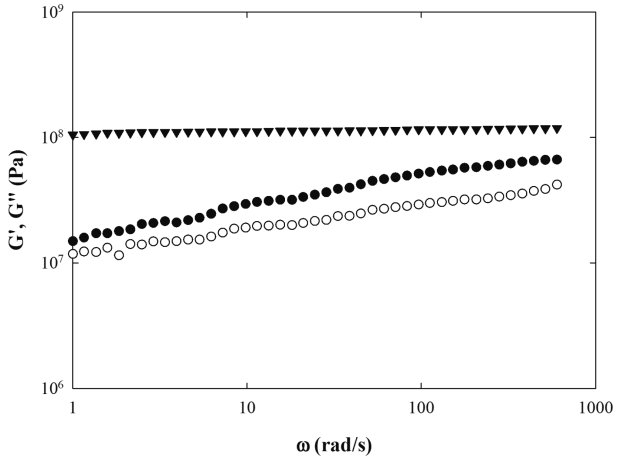

Figure 2. Elastic (G', black symbols) and viscous (G'', white symbols) moduli vs angular frequency, at 273.15 K and 0.005% strain, for $HMIm(PFBu)SO_3$ (circles) and $NB_4(PFBu)SO_3$ (triangles). The uncertainty value in the determination of elastic and viscous moduli is 6% (see Figure S3).

In the case of $NB_4(PFBu)SO_3$, Figure 1d shows a different behavior than that of the first. The temperature ramp shows a single and clear solid−fluid transition, with no other singular points detected, according to the diagram shown by DSC. It is evident that it is the cation that produces this different trend, and NB_4^+ does not present the preferentially elongated conformation which, in the case of $HMIm^+$, might induce the effects shown. The solid phase also makes an important difference, as Figure 2 shows only G', with a fairly constant trend against angular frequency, typical of a crystalline solid.

In order to ascertain the Newtonian behavior of the FILs under study in the liquid state, a constant temperature rheological study was carried out, at 313.15 K for $HMIm(PFBu)SO_3$ and at 363.15 K for $NB_4(PFBu)SO_3$. The most direct method for determining whether a fluid is Newtonian or not is to perform a rotational study or flux test. At constant temperature the shear stress is varied following a logarithmic scale. If the fluid is Newtonian, the shear viscosity must demonstrate an independent shear rate trend. Figure 3a shows that, for both FILs, but especially for $NB_4(PFBu)SO_3$, viscosity seems to decrease at low shear rate values. This trend alone could lead to a mistaken conclusion of non-Newtonian behavior. However, it may be explainable by the sensitivity limit of the rheometer, due to limiting low torque values. Therefore, an oscillatory test was performed within the linear viscoelastic range (LVR) to distinguish between the possible origins of this trend. A frequency sweep test was carried out at constant temperature; for a Newtonian fluid this should yield constant complex viscosity, whose value should be similar to that shown by the shear viscosity measured in the previous test at similar temperatures, angular frequency, and shear rates.[37] Figure 3b shows the results of this test, with constant complex viscosity values (Newtonian behavior) at frequencies ranging from 1.5 to 50 rad s^{-1} (see Table S3). Above this range, problems of inertia appear while below it the mentioned torque limitations become evident, showing the rheometer detection limits. If we compare the angular frequency 10 rad s^{-1}, which corresponds approximately to a shear rate of 10 s^{-1} in the flux

dx.doi.org/10.1021/jp402300c | J. Phys. Chem. B 2013, 117, 10826−10833

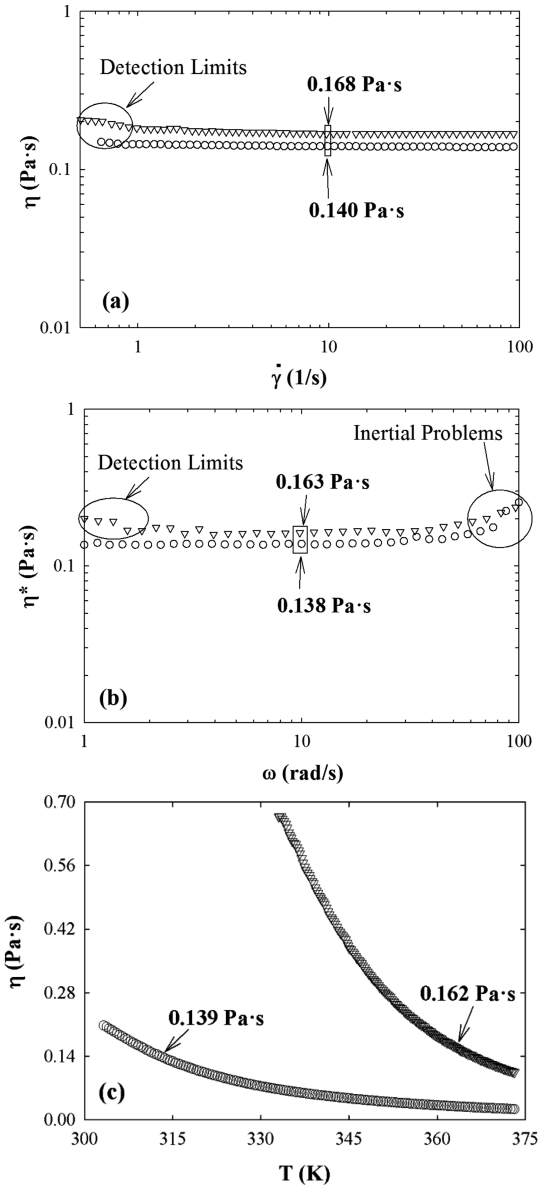

Figure 3. (a) Viscosity vs shear rate and (b) complex viscosity vs angular frequency for HMIm(PFBu)SO_3 at 313.15 K (circles) and NB_4(PFBu)SO_3 at 363.15 K (inverted triangles). (c) Viscosity variation vs temperature at 10 s^{-1}, symbols legend as before. The uncertainty value in the determination of viscosity is 3% (see Figure S4).

test, the viscosity values are compatible within the estimated uncertainty value in the determination of viscosity in this range, which is 3%, which evidence the Newtonian behavior of both FILs within the range studied.

Finally, temperature ramps were performed for both FILs at the same heating rates as the other rheological tests and with a constant shear rate value of 10 s^{-1}. These results are plotted in Figure 3c showing that, for each FIL, the viscosity values for a given temperature and shear rate match exactly those found previously; this test of consistency is, thus, concluded.

Molecular Dynamic (MD) Simulations. The interpretation of the experimental data at a molecular and structural level was performed using molecular dynamics (MD) simulations. These were carried out in the liquid phase of the pure ILs, and the results were used to infer the possible nature of the underlying crystallization processes. Such a procedure is warranted, on the one hand, due to the highly structured nature of ionic liquids whose complexity must be partially maintained (and augmented) during crystallization and, on the other, due to the difficulty in implementing simulation techniques to explicitly model the solid−liquid equilibria (e.g., Gibbs ensemble Monte Carlo methods[38]) in such dense media.

In order to compare the influence of the fluorous chain on the structure of the ionic liquids, we also analyzed the hydrogenated counterparts of HMIm(PFBu)SO_3 and NB_4(PFBu)SO_3, i.e., the HMImBuSO_3 and NB_4BuSO_3 systems.

Figure 4 shows the pair radial distribution functions corresponding to the interaction centers representative of the

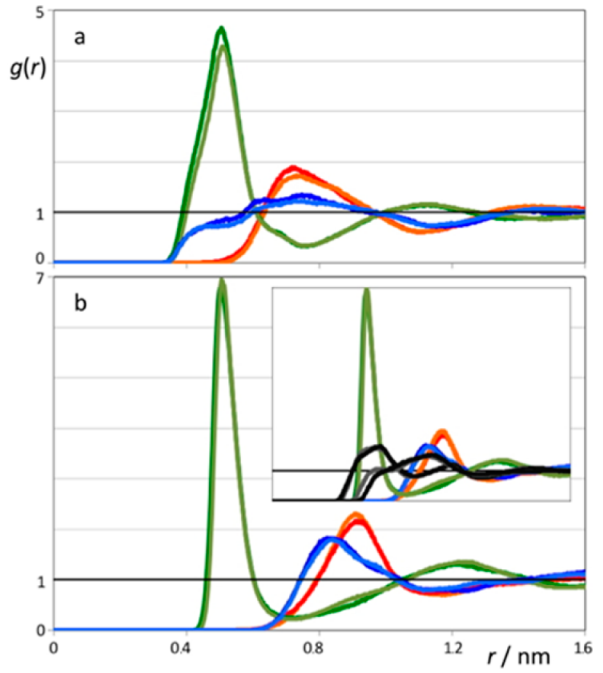

Figure 4. Pair radial distribution functions (RDFs) between selected interaction centers of (a) HMIm-based and (b) NB_4-based ILs. Green, red, and blue RDFs represent correlations between anion−cation, anion−anion, and cation−cation charged centers, respectively. The inset in (b) also shows (nonpolar)-ion correlations in black. The selected atoms/centers are highlighted in bold and underlined; **Im** represents the centroid of the imidazolium ring; **B_4** and **Bu** represent the carbon atoms of the methyl groups of the tetraalkylammonium cation and alkylsulfonate anions, respectively. (a) Light green = HM**Im**-Bu**S**O_3; dark green = HM**Im**-(PFBu)**S**O_3; dark/light blue = HM**Im**-HM**Im** in fluorinated/hydrogenated IL; red = (PFBu)**S**O_3-(PFBu)**S**O_3; orange = Bu**S**O_3-Bu**S**O_3; (b) light green = **N**B_4-Bu**S**O_3; dark green = **N**B_4-(PFBu)**S**O_3; dark/light blue = **N**B_4-**N**B_4 in fluorinated/hydrogenated IL; red = (PFBu)**S**O_3-(PFBu)**S**O_3; orange = Bu**S**O_3−Bu**S**O_3; (inset) the same as (b) plus gray/black = N**B$_4$**-Bu**S**O_3 and **N**B_4- **Bu**SO_3 in hydrogenated/fluorinated ILs.

charged parts of the ions. The figure shows the usual opposition-of-phase behavior between the anion−cation RDFs and the (cation−cation or anion−anion) RDFs (e.g., crossovers at 0.6, 0.95, and 1.3 nm for HMIm-based systems). Such a pattern is typical for charged systems exhibiting intermediate-range ordering due to the local electroneutral conditions imposed by Coulomb interactions.[39] It also reflects the existence of a polar network formed by the charged centers

dx.doi.org/10.1021/jp402300c | J. Phys. Chem. B 2013, 117, 10826−10833

of the ions at contact distances permeating the entire liquid media. Since the RDFs were obtained using the centers-of also reflects the existence of a polar network formed by the charger centers of the ions at contact distances permeating the entire liquid media.[40]

There is, however, an important structural difference between the two ionic liquids under discussion: the HMIm-based ones show a polar network whose connectivity spans the entire distance range while their NB_4-based counterparts show a "gap" between 0.6 and 0.7 nm (Figure 4b). This difference demonstrates how the connectivity of the polar network and the formation of nanosegregated domains can be affected by the morphology of the underlying ions: anisotropic and more exposed centers of charge in the case of the 1-hexyl-3-methylimidazolium cation. There is a central and concealed center of charge in the case of the tetrabutylammonium cation. The latter arrangement implies that the polar network will be partially encased by butyl groups—in fact, the corresponding polar−(nonpolar) RDFs fill the above-mentioned "gap", as shown in the inset of Figure 4b.

The difference between the two types of cation can also be seen in Figure 5 where snapshots of the simulation boxes are shown along with the calculated structure factors.

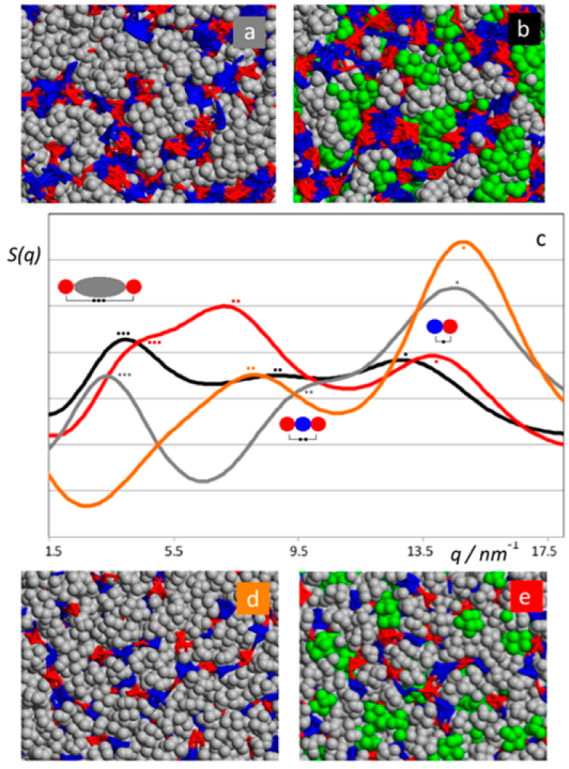

Figure 5. MD simulation snapshots (a, b, d, e) and total static structure factors (c), $S(q)$, for the HMIm $BuSO_3$ (a, gray), $HMIm(PFBu)SO_3$ (b, black), NB_4BuSO_3 (orange, d), and $NB_4(PFBu)SO_3$ (red, e) systems. The scales in all snapshots are the same. The dots in (c) represent the relations between the different q peaks/shoulders and the characteristic distances between charged centers in the polar networks of the ionic liquids. Gray curve peaks: 14.5 nm^{-1} (single dot), 9.8 nm^{-1} (double dot), 3.3 nm^{-1} (triple dot). Black curve peaks: 12.9 nm^{-1} (single dot), 8.8 nm^{-1} (double dot), 4.0 nm^{-1} (triple dot). Orange curve peaks: 14.8 nm^{-1} (single dot), 8.1 nm^{-1} (double dot). Red curve peaks: 13.8 nm^{-1} (single dot), 7.1 nm^{-1} (double dot), 4.3 nm^{-1} (triple dot).

The differences between the polar networks (red/blue) of the different systems can be evaluated by the comparison of Figures 5a,b or Figures 5d,e: (i) the more developed (bulkier) polar network of the $HMIm^+$ systems contrasts with the string-like polar domains of the NB_4^+ systems; (ii) the former network is effectively segregated from the alkyl nonpolar domains while the latter is encased by the (sheathing) butyl groups of the cation.

The structure factors of C_nMIm-based ionic liquids (namely in the C_nMIm $N(SO_2CF_3)_2$ and C_nMIm PF_6 series) have been discussed at length.[39,41] The $S(q)$ function of HMIm $BuSO_3$ shows the usual three peaks/shoulders at q values of 14, 10, and 3 nm^{-1} corresponding in reciprocal space to distances between contact ion pairs (+)(−), equally charged ions in the polar network (+/−)(−/+)(+/−), and ions separated by nonpolar domains (+/−)(nonpolar)(+/−), respectively. On the other hand, the NB_4 $BuSO_3$ $S(q)$ function shows only two peaks at q = 15 and 8 nm^{-1}. The absence of a so-called prepeak in the 2−4 nm^{-1} range implies the inexistence of effective polar/nonpolar segregation due to the presence of the butyl groups that must surround the charged center of the cation. The encasing of the polar network also justifies the shift in the reciprocal distances between the equally charged ions in the polar network from 10 to 8 nm^{-1}.

When the alkyl chains of the anions are fluorous the distances between the ion contact pairs increase slightly (the q values decrease from 14 and 15 nm^{-1} to 13 and 14 nm^{-1} in the HMIm- and NB_4-based systems, respectively), reflecting a bulkier environment near the charged head of the anion. The same applies to the distances between equally charged ions in the polar network (decrease from 10 and 8 nm^{-1} to 9 to 7 nm^{-1}). However, the most interesting features of the new set of $S(q)$ functions are the appearance of a shoulder around 4−5 nm^{-1} in the $NB_4(PFBu)SO_3$ and the flattening of the valley in the 6 nm^{-1} region when one considers $HMIm(PFBu)SO_3$ instead of $HMImBuSO_3$. This suggests that the fluorination of the alkyl side chain of one of the ions appears to increase the level of segregation in the HMIm-based systems (the gray and green areas do not mix in Figure 5b) and start it in the case of $NB_4(PFBu)SO_3$ (Figure 5e).

The overall $S(q)$ functions and the corresponding snapshots of Figure 5 also provide a possible explanation for the different behavior of the two FILs upon freezing: the three types of domain (polar, hydrogenated, fluorous) will be able to adopt different relative positions in a crystal of $HMIm(PFBu)SO_3$—think of the red/blue, gray, and green domains in Figure 5b as three interchangeable jigsaw pieces. On the other hand, in $NB_4(PFBu)SO_3$, the polar (red/blue) and hydrogenated (gray) regions are interlocked and, together with the incipient fluorous domains (green), thus face a very limited number of crystallization options.

CONCLUSIONS

In conclusion, the two fluorinated ionic liquids, $HMIm(PFBu)SO_3$ and $NB_4(PFBu)SO_3$, provide valuable insights into the possible formation of three nanosegregated domains: polar, nonpolar, and fluorous. The characterization of these two FILs was carried out using differential scanning calorimetry and rheology techniques which allow us to identify and locate the solid−fluid transitions of these two FILs and their dynamic and thermodynamic behavior. In these experimental data, the appearance of solid−solid transitions in $HMIm(PFBu)SO_3$ strongly supports the hypothesis of a nanostructure in this

dx.doi.org/10.1021/jp402300c | J. Phys. Chem. B 2013, 117, 10826−10833

FIL. In the case of $NB_4(PFBu)SO_3$, this FIL is also a nanostructured ionic liquid, but the symmetry of cation could be the reason for impeding the formation of different types of crystal. The repulsion between perfluorinated and aliphatic chains, which tend to group separately, could be the underlying reason for this rich phase scenario. Finally, the simulations results demonstrate the formation of three nanosegregated domains—polar, nonpolar, and fluorous—that may be able to adopt different relative positions in a crystal of HMIm $(PFBu)SO_3$ inducing the observed calorimetry and rheological results. These three mesoscopic domains could act as interchangeable jigsaw pieces enabling the formation of multiple types of crystals.

■ ASSOCIATED CONTENT

Supporting Information

Chemical structures of the fluorinated ionic liquids studied in this work and thermal properties obtained using differential scanning calorimetry. This material is available free of charge via the Internet at http://pubs.acs.org.

■ AUTHOR INFORMATION

Corresponding Authors

*E-mail anab@itqb.unl.pt; Fax +351 214411277; Tel +351 214469414 (A.B.P.).

*E-mail jnlopes@ist.utl.pt; Fax +351 214411277; Tel +351 214469419 (J.N.C.L.).

Notes

The authors declare no competing financial interest.

■ ACKNOWLEDGMENTS

Financial support for this project was provided by Fundação para a Ciência e Tecnologia (FCT) through project PTDC/EQU-FTT/118800/2010. A. B. Pereiro acknowledges Marie Curie Actions Intra-European Fellowships (IEF) for a contract under FP7-PEOPLE-2009-IEF-252355-HALOGENILS and for financial support of FCT/MCTES (Portugal) by way of a Post-Doctoral grant SFRH/BPD/84433/2012. K. Shimizu and I. M. Marrucho acknowledge FCT/MCTES (Portugal) for the Post-Doctoral grant SFRH/BPD/38339/2007 and a contract under Programa Ciência 2007, respectively. M. M. Piñeiro acknowledges the Xunta de Galicia (Spain) for Galician Network on Ionic Liquids, REGALIs (CN 2012/120). Furthermore, the authors acknowledge Carlos Gracia (TA Instruments) for his help in the interpretation of the DSC experimental data.

■ REFERENCES

(1) Banks, R. E.; Smart, B. E.; Tatlow, J. C. *Organofluorine Chemistry – Principles and Commercial Applications*; Plenum Press: New York, 1994.

(2) Riess, J. G. Oxygen Carriers ("Blood Substitutes")-Raison d'Etre, Chemistry, and Some Physiology. *Chem. Rev.* **2001**, *101*, 2797–2919.

(3) Eckert, C. A.; Knutson, B. L.; Debenedetti, P. G. Supercritical Fluids as Solvents for Chemical and Materials Processing. *Nature* **1996**, *383*, 313–318.

(4) de Melo, M. J. P.; Dias, A. M. A.; Blesic, M.; Rebelo, L. P. N.; Vega, L. F.; Coutinho, J. A. P.; Marrucho, I. M. Liquid-Liquid Equilibrium of (Perfluoroalkane plus Alkane) Binary Mixtures. *Fluid Phase Equilib.* **2006**, *242*, 210–219.

(5) Gomes, M. F. C.; Padua, A. A. H. Interactions of Carbon Dioxide with Liquid Fluorocarbons. *J. Phys. Chem. B* **2003**, *107*, 14020–14024.

(6) Shen, Y.; Kennedy, D. F.; Greaves, T. L.; Weerawardena, A.; Mulder, R. J.; Kirby, N.; Song, G. H.; Drummond, C. J. Protic Ionic Liquids with Fluorous Anions: Physicochemical Properties and Self-assembly Nanostructure. *Phys. Chem. Chem. Phys.* **2012**, *14*, 7981–7992.

(7) Greaves, T. L.; Kennedy, D. F.; Shen, Y.; Hawley, A.; Song, G. H.; Drummond, C. J. Fluorous Protic Ionic Liquids Exhibit Discrete Segregated Nano-scale Solvent Domains and Form New Populations of Nano-scale Objects upon Primary Alcohol Addition. *Phys. Chem. Chem. Phys.* **2013**, *15*, 7592–7598.

(8) Xue, H.; Shreeve, J. M. Ionic Liquids with Fluorine-Containing Cations. *Eur. J. Inorg. Chem.* **2005**, 2573–2580.

(9) Tsukada, Y.; Iwamoto, K.; Furutani, H.; Matsushita, Y.; Abe, Y.; Matsumoto, K.; Monda, K.; Hayase, S.; Kawatsura, M.; Itoh, T. Preparation of Novel Hydrophobic Fluorine-substituted-alkyl Sulfate Ionic Liquids and Application as an Efficient Reaction Medium for Lipase-catalyzed Reaction. *Tetrahedron Lett.* **2006**, *47*, 1801–1804.

(10) Arvai, R.; Toulgoat, F.; Medebielle, M.; Langlois, B.; Alloin, F.; Iojoiu, C.; Sanchez, J. Y. J. New Aryl-Containing Fluorinated Sulfonic Acids and Their Ammonium Salts, Useful as Electrolytes for Fuel Cells or Ionic Liquids. *Fluorine Chem.* **2008**, *129*, 1029–1035.

(11) Linder, T.; Sundermeyer, J. Three Novel Anions Based on Pentafluorophenyl Amine Combined with Two New Synthetic Strategies for the Synthesis of Highly Lipophilic Ionic Liquids. *Chem. Commun.* **2009**, 2914–2916.

(12) Skalicky, M.; Rybackova, M.; Kysilka, O.; Kvicalova, M.; Cvacka, J.; Cejka, J.; Kvicala, J. Synthesis of Bis(polyfluoroalkylated)-imidazolium Salts as Key Intermediates for Fluorous NHC Ligands. *J. Fluorine Chem.* **2009**, *130*, 966–973.

(13) Tindale, J. J.; Mouland, K. L.; Ragogna, P. J. Thiol Appended, Fluorinated Phosphonium Ionic Liquids as Covalent Superhydrophobic Coatings. *J. Mol. Liq.* **2010**, *152*, 14–18.

(14) Livi, S.; Duchet-Rumeau, J.; Gerard, J. F. Tailoring of Interfacial Properties by Ionic Liquids in a Fluorinated Matrix Based Nanocomposites. *Eur. Polym. J.* **2011**, *47*, 1361–1369.

(15) Ganapatibhotla, L. V. N. R.; Wu, L.; Zheng, J. P.; Jia, X. L.; Roy, D.; McLaughlin, J. B.; Krishnan, S. Ionic Liquids with Fluorinated Block-oligomer Tails: Influence of Self-assembly on Transport Properties. *J. Mater. Chem.* **2011**, *21*, 19275–19285.

(16) Smith, G. D.; Borodin, O.; Magda, J. J.; Boyd, R. H.; Wang, Y.; Bara, J. E.; Miller, S.; Gin, D. L.; Noble, R. D. A Comparison of Fluoroalkyl-derivatized Imidazolium:TFSI and Alkyl-derivatized Imidazolium:TFSI Ionic Liquids: A Molecular Dynamics Simulation Study. *Phys. Chem. Chem. Phys.* **2010**, *12*, 7064–7076.

(17) Holbrey, J. D.; Reichert, W. M.; Rogers, R. D. Crystal Structures of Imidazolium Bis(trifluoromethanesulfonyl)imide 'Ionic Liquid' Salts: The First Organic Salt with a cis-TFSI Anion Conformation. *Dalton Trans.* **2004**, 2267–2271.

(18) Lopes, J. N. A. C.; Pádua, A. A. H. Nanostructural Organization in Ionic Liquids. *J. Phys. Chem. B* **2006**, *110*, 3330–3335.

(19) Triolo, A.; Russina, O.; Bleif, H. J.; Di Cola, E. Nanoscale Segregation in Room Temperature Ionic Liquids. *J. Phys. Chem. B* **2007**, *111*, 4641–4644.

(20) Triolo, A.; Russina, O.; Fazio, B.; Triolo, R.; Di Cola, E. Morphology of 1-Alkyl-3-methylimidazolium Hexafluorophosphate Room Temperature Ionic Liquids. *Chem. Phys. Lett.* **2008**, *457*, 362–365.

(21) Greaves, T. L.; Kennedy, D. F.; Mudie, S. T.; Drummond, C. J. Diversity Observed in the Nanostructure of Protic Ionic Liquids. *J. Phys. Chem. B* **2010**, *114*, 10022–10031.

(22) Greaves, T. L.; Kennedy, D. F.; Weerawardena, A.; Tse, N. M. K.; Kirby, N.; Drummond, C. J. Nanostructured Protic Ionic Liquids Retain Nanoscale Features in Aqueous Solution While Precursor Bronsted Acids and Bases Exhibit Different Behavior. *J. Phys. Chem. B* **2011**, *115*, 2055–2066.

(23) Pott, T.; Meleard, P. New Insight into the Nanostructure of Ionic Liquids: A Small Angle X-ray Scattering (SAXS) Study on Liquid Tri-alkyl-methyl-ammonium Bis(trifluoromethanesulfonyl)amides and Their Mixtures. *Phys. Chem. Chem. Phys.* **2009**, *11*, 5469–5475.

(24) Hayes, R.; El Abedin, S. Z.; Atkin, R. Pronounced Structure in Confined Aprotic Room-Temperature Ionic Liquids. *J. Phys. Chem. B* **2009**, *113*, 7049–7052.

(25) Lopes, J. N. C.; Gomes, M. F. C.; Pádua, A. A. H. Nonpolar, Polar, and Associating Solutes in Ionic Liquids. *J. Phys. Chem. B* **2006**, *110*, 16816−16818.
(26) Takamuku, T.; Tobiishi, M.; Saito, H. Solvation Properties of Aliphatic Alcohol−Water and Fluorinated Alcohol−Water Solutions for Amide Molecules Studied by IR and NMR Techniques. *J. Solution Chem.* **2011**, *40*, 2046−2056.
(27) Pastoriza-Gallego, M. J.; Lugo, L.; Legido, J. L.; Piñeiro, M. M. Rheological Non-Newtonian Behaviour of Ethylene Glycol-Based Fe_2O_3 Nanofluids. *Nanoscale Res. Lett.* **2011**, *6*, 560.
(28) Canongia Lopes, J. N.; Deschamps, J.; Pádua, A. A. H. Modeling Ionic Liquids Using a Systematic All-Atom Force Field. *J. Phys. Chem. B* **2004**, *108*, 2038−2047.
(29) Canongia Lopes, J. N.; Pádua, A. A. H. Molecular Force Field for Ionic Liquids Composed of Triflate or Bistriflylimide Anions. *J. Phys. Chem. B* **2004**, *108*, 16893−16898.
(30) Canongia Lopes, J. N.; Pádua, A. A. H.; Shimizu, K. Molecular Force Field for Ionic Liquids IV: Trialkylimidazolium and Alkoxycarbonyl-Imidazolium Cations; Alkylsulfonate and Alkylsulfate Anions. *J. Phys. Chem. B* **2008**, *112*, 5039−5046.
(31) Smith, W.; Forester, T. R.; Todorov, I. T. *The DL-POLY 2 User Manual, Version 2.20*; STFC Daresbury Laboratory: Warrington, UK., 2009.
(32) Du, J.; Benmore, C. J.; Corrales, R.; Hart, R. T.; Richard Weber, J. K. A Molecular Dynamics Simulation Interpretation of Neutron and X-ray Diffraction Measurements on Single Phase Y_2O_3−Al_2O_3 Glasses. *J. Phys.: Condens. Matter* **2009**, *21*, 205102.
(33) Faria, L. F. O.; Matos, J. R.; Ribeiro, M. C. C. Thermal Analysis and Raman Spectra of Different Phases of the Ionic Liquid Butyltrimethylammonium Bis(trifluoromethylsulfonyl)imide. *J. Phys. Chem. B* **2012**, *116*, 9238−9245.
(34) Nishikawa, K.; Tozaki, K. I. Intermittent Crystallization of an Ionic Liquid: 1-Isopropyl-3-methylimidazolium Bromide. *Chem. Phys. Lett.* **2008**, *463*, 369−372.
(35) Nishikawa, K.; Wang, S.; Tozaki, K. I. Rhythmic Melting and Crystallizing of Ionic Liquid 1-Butyl-3-methylimidazolium Bromide. *Chem. Phys. Lett.* **2008**, *458*, 88−91.
(36) Russina, O.; Triolo, A.; Gontrani, L.; Caminiti, R.; Xiao, D.; Hines, L. G.; Bartsch, R. A.; Quitevis, E. L.; Pleckhova, N.; Seddon, K. R. Morphology and Intermolecular Dynamics of 1-Alkyl-3-methylimidazolium bis{(trifluoromethane)sulfonyl}amide Ionic Liquids: Structural and Dynamic Evidence of Nanoscale Segregation. *J. Phys.: Condens. Matter* **2009**, *21*, 424121.
(37) Cox, W. P.; Merz, E. H. Correlation of Dynamic and Steady-Flow Viscosities. *J. Polym. Sci.* **1958**, *28*, 619.
(38) Canongia Lopes, J. N.; Tildesley, D. J. Multiphase Equilibria using the Gibbs Ensemble Monte Carlo Method. *Mol. Phys.* **1997**, *92*, 187−195.
(39) Annapureddy, H. V. R.; Kashyap, H. K.; De Biase, P. M.; Margulis, C. J. What Is the Origin of the Prepeak in the X-ray Scattering of Imidazolium-Based Room-Temperature Ionic Liquids? *J. Phys. Chem. B* **2010**, *114*, 16838−16846.
(40) Padua, A. A. H.; Gomes, M. F.; Lopes, J. N. A. C. Molecular Solutes in Ionic Liquids: A Structural, Perspective. *Acc. Chem. Res.* **2007**, *40*, 1087−1096.
(41) Russina, O.; Triolo, A. New Experimental Evidence Supporting the Mesoscopic Segregation Model in Room Temperature Ionic Liquids. *Faraday Discuss.* **2012**, *154*, 97−109.